Journal of Molecular Catalysis A: Chemical 349 (2011) 71–79

Contents lists available at SciVerse ScienceDirect

Journal of Molecular Catalysis A: Chemical

journal homepage: www.elsevier.com/locate/molcata

p-Nitrophenol degradation by a heterogeneous Fenton-like reaction on nano-magnetite: Process optimization, kinetics, and degradation pathways

Sheng-Peng Sun, Ann T. Lemley*

Graduate Field of Environmental Toxicology, Cornell University, 209 MVR Hall, Ithaca, NY 14853, United States

ARTICLE INFO

Article history:
Received 8 July 2011
Received in revised form 23 August 2011
Accepted 25 August 2011
Available online 2 September 2011

Keywords:
p-Nitrophenol
Heterogeneous Fenton-like reaction
Nano-Fe_3O_4
Hydroxyl radical
Response surface methodology
Kinetics

ABSTRACT

Heterogeneous Fenton-like reactions on nano-magnetite (Fe_3O_4) were investigated for the degradation of p-Nitrophenol (p-NP). A four factor central composite design (CCD) coupled with response surface methodology (RSM) was applied to evaluate and optimize the important variables. A significant quadratic model (P-value < 0.0001, R^2 = 0.9442) was derived using analysis of variance (ANOVA), which was adequate to perform the process variables optimization. Optimum conditions were determined to be 1.5 g L^{-1} Fe_3O_4, 620 mM H_2O_2, pH 7.0 and 25–45 mg L^{-1} p-NP. More than 90% of p-NP was experimentally degraded after 10 h of reaction time under the optimum conditions, which agreed well with the model predictions. The results demonstrated that the degradation of p-NP was due to the attack of hydroxyl radicals (•OH) generated by the surface-catalyzed decomposition of hydrogen peroxide on the nano-Fe_3O_4, i.e. heterogeneous Fenton-like reactions. Possible mechanisms of p-NP degradation in this system were proposed, based on intermediates identified by LC–MS and GC–MS and included benzoquinone, hydroquinone, 1,2,4-trihydroxybenzene and p-nitrocatechol. The kinetic analysis implied that the generation rate of •OH ($V_{•OH}$) was increased along with the degradation of p-NP. This was attributed to the formation of acidic products, which decreased the solution pH and enhanced the decomposition of absorbed hydrogen peroxide via a radical producing pathway on the nano-Fe_3O_4 surface.

© 2011 Elsevier B.V. All rights reserved.

1. Introduction

p-Nitrophenol (p-NP) is an important chemical that is being widely used as a precursor or intermediate for the preparation of pesticides, insecticides, herbicides, explosives, synthetic dyes and pharmaceuticals. However, p-NP has been listed as a priority pollutant by the U.S. EPA due to its toxicity, both potential carcinogenic and mutagenic effects [1]. The strong electro-withdrawing effect of the nitro group ($-NO_2$) in the aromatic ring of p-NP enhances its stability to resist chemical and biological oxidation, but the anaerobic degradation of p-NP can produce nitroso and aromatic amines which cannot be regarded as environmentally safe end products [2]. Because of its stability and high solubility (11.6 g L^{-1}, 20 °C), p-NP can persist a very long time in the soil and ground water and pose a significant environmental risk.

Advanced oxidation processes (AOPs) have attracted considerable attention in the past decade; the generation of highly reactive and non-selective hydroxyl radicals (·OH) can oxidize and mineralize most organic compounds at near diffusion-limited rates, especially unsaturated organic compounds [3]. Heterogeneous Fenton-like reactions on solid catalysts can effectively catalyze the oxidation of organic pollutants at neutral or nearly neutral pH conditions, which is beneficial for *in situ* remediation of polluted groundwater and soils [4]. Iron-based clays, silicas and zeolites, resin supported ferrous and ferric species, iron containing ashes and iron oxide minerals are capable of serving as heterogeneous Fenton-like catalysts [4–9]. Among these catalysts, iron oxide minerals attract more attention, because they are widespread in the natural environment and can be easily applied to *in situ* remediation processes.

Magnetite (Fe_3O_4) is a mixed-valence iron oxide with unique redox properties. It can form naturally via several pathways including iron metal corrosion, ferrous species oxidation, and chemical and biological reduction of ferric species [10]. Because Fe_3O_4 is a common constituent of soils and sediments, it can be potentially considered as an environmentally benign material for the decontamination of polluted waters and soils. Researchers have shown that Fe_3O_4 can be implicated as a potentially important reductant of environmental contaminants, including halogenated organics carbon tetrachloride, tetrachloroethylene, trichloroethylene, 1,1-dichloroethylene, cis-1,2-dichloroethylene and vinyl chloride [11–13]; aromatic nitro compounds nitrobenzene and 2,4,6-trinitrotoluene [10,14]; and heavy metals mercury (Hg^{2+}), chromium (Cr^{6+}) and uranium (U^{6+}) [15–17]. The reductive degradation of organic compounds by Fe_3O_4 potentially transforms the target compounds to less hazardous or more biodegradable

* Corresponding author. Tel.: +1 607 255 3151; fax: +1 607 255 1093.
E-mail address: ATL2@cornell.edu (A.T. Lemley).

1381-1169/$ – see front matter © 2011 Elsevier B.V. All rights reserved.
doi:10.1016/j.molcata.2011.08.022

products, but cannot lead to the mineralization of them. On the contrary, complete degradation and partial mineralization of organic pollutants can be achieved by the heterogeneous Fenton-like reactions due to the generation of highly reactive •OH. The Fe^{2+} probably plays an important role to enhance the production rate of ·OH, which might be reversibly oxidized and reduced in the same structure due to the octahedral sites of the magnetite structure [18]. Fe_3O_4 as a heterogeneous Fenton-like catalyst is more effective than other iron oxide minerals such as ferrihydrite, hematite, goethite and lepidocrocite [4]. Most recently, we reported the successful removal of a pesticide 4,6-dinitro-o-cresol (DNOC) using nano-Fe_3O_4 as the iron source and cathodic generation of hydrogen peroxide [19]. However, it was found that the homogeneous Fenton reactions and direct electrolysis were the major processes for the degradation of DNOC at acid and near neutral pH, respectively. The heterogeneous Fenton reactions were not obvious probably because of the small generation rate of hydrogen peroxide (1.45×10^{-2} mM min^{-1}).

The degradation of p-NP by heterogeneous Fenton-like reactions on Fe_3O_4 has not yet been reported in the literature. The use of nanoparticles as catalysts is more attractive than that of microparticles because they normally show higher catalytic activity due to their large specific surface area. Therefore, the aim of the present study is to investigate heterogeneous Fenton-like reactions on nano-Fe_3O_4 for p-NP degradation in water. The degradation efficiency of pollutants by this process basically depends on catalyst dosage, hydrogen peroxide concentration, the initial pH and the initial concentration of pollutants. The traditional method to determine the optimal conditions of these variables is to test a single factor at one time while keeping the other variables constant. This methodology does not include a study of interactions between variables and could lead to restricted conclusions. A better research plan should include selection of the variables involved in the process, factorial design of experiments, experimental assays and fitting of results using mathematical methods. Central composite design (CCD) coupled with response surface methodology (RSM) is a useful approach for optimizing variables that has been used successfully in other studies [20–22]. The objectives of this study were (i) to evaluate and optimize the important variables for p-NP degradation using CCD and RSM; (ii) to quantify the contributions of homogeneous and heterogeneous reactions on p-NP degradation and to identify the primary reactive species; (iii) to investigate the degradation kinetics of p-NP and better understand the related reaction mechanisms; and (iv) to determine the intermediate products and discuss the possible pathways of p-NP degradation.

2. Experimental

2.1. Materials

p-NP was obtained from Aldrich Chemical Company, Inc. (Milwaukee, USA). Hydrogen peroxide (30%, w/w), ammonium acetate, hydrochloric acid, hydroxylamine hydrochloride, sodium sulfate anhydrous, sulfuric acid, 2-propanol, chloroform, dichloromethane and ethyl acetate were obtained from Mallinckrodt Baker, Inc. (Phillipsburg, USA). Iron standard solution (10 mg L^{-1} Fe) was obtained form HACH Company (Loveland, USA). 1,10-phenanthroline monohydrate solution (0.1%) was obtained from Labchem Inc. (Pittsburgh, USA). Ammonium molybdate (VI) tetrahydrate was obtained from Acros Organics Company (New Jersey, USA). Potassium hydrogen phthalate, sodium hydroxide, HPLC grade methanol and pure water were obtained from Fisher Scientific Company (Fair Lawn, USA). All chemicals were analytical grade reagents and were used as received without further purification. Distilled, deionized water was used for the preparation of solutions.

Nano-Fe_3O_4 was obtained from Nanostructured & Amorphous Materials Inc. (Texas, USA). The characterization of the nano-Fe_3O_4 has been reported in our recent publication [19]. The average diameter of the nano-Fe_3O_4 was determined to be 30 nm by scanning electron microscopy (SEM, HITACHIFEG 54800) and transmission electron microscopy (TEM, Philips CM20). The specific surface area was measured to be 48 ± 2 m^2 g^{-1} using a Coulter SA3100 surface area analyzer.

Table 1
Variable levels of CCD for the degradation of p-NP by heterogeneous Fenton-like reactions on nano-Fe_3O_4.

Process variables	Symbol	Actual values of the coded variable levels				
		−2	−1	0	1	2
Fe_3O_4 (g L^{-1})	X_1	0.2	0.6	1	1.4	1.8
H_2O_2 (mM)	X_2	10	205	400	595	790
pH	X_3	5.0	6.0	7.0	8.0	9.0
$C_{p\text{-}NP}$ (mg L^{-1})	X_4	5	15	25	35	45

2.2. Experimental design with RSM

A central composite design (CCD) with four factors and five coded levels was used for the experimental design. Table 1 shows the experimental ranges and levels of the independent variable tested in the CCD. The variables X_i were coded as x_i according to the following equation (Eq. (1)):

$$x_i = \frac{X_i - X_{i,0}}{\delta X_i} \quad (i = 1, 2, \ldots, 4) \tag{1}$$

where X_i is the real value of the independent variable, $X_{i,0}$ is the value of X_i at the center point of the investigated area and the δX_i is the step change. The loading dosages of nano-Fe_3O_4 (X_1) and hydrogen peroxide (X_2), initial pH (X_3) and initial concentration of p-NP (X_4) were chosen as the independent input variables. The degradation efficiency of p-NP (Y) was used as the dependent output variable. The response variable was fitted by a quadratic polynomial equation (Eq. (2)):

$$Y = b_0 + \sum_{i=1}^{n} b_i x_i + \sum_{i=1}^{n} b_{ii} x_i^2 + \sum_{i=1}^{n-1} \sum_{j=i+1}^{n} b_{ij} x_i x_j \tag{2}$$

where Y represents the predicted the degradation efficiency of p-NP (%), b_0 is the offset term (constant), b_i are the linear coefficients, b_{ii} are the quadratic coefficients, b_{ij} are the interaction coefficients, and x_i and x_j are the code values of the independent input variables.

2.3. Experimental procedures

Batch experiments were carried out in 50 ml polypropylene conical centrifuge tubes (30×115 mm). Typically, an appropriate concentration of p-NP solution was prepared by diluting the stock p-NP solution with distilled, deionized water. The pH of the p-NP solution was adjusted to a desired value using 0.1 M sulfuric acid and 0.1 M sodium hydroxide. Following the pH adjustment, an appropriate dosage of nano-sized Fe_3O_4 was mixed with 25 ml prepared p-NP solution in a 30 ml glass bottle, and the mixture was subjected to ultrasonic irradiation for 5 min in an ultrasound bath (100 W, 42 kHz, Branson 2510R-DTH). After that, the mixture was transferred to a 50 ml centrifuge tube and then was filled to 50 ml with the prepared p-NP solution. The centrifuge tube was then shaken for 1 h to allow the physical adsorption of p-NP molecules on nano-Fe_3O_4 particles reaching equilibrium. It is noteworthy that

the degradation of p-NP during the ultrasonic dispersion process and physical adsorption on nano-Fe_3O_4 was lower than 2%, which can be neglected (some samples were held for 3 days and checked for concentration to verify that volatilization did not occur). Subsequently, the Fenton-like reaction was started by the addition of the appropriate amount of hydrogen peroxide. For the specific radical scavenging experiments, an appropriate amount of scavenger was added to the solutions prior to the addition of hydrogen peroxide. To identify the major aromatic intermediates, a high initial concentration of p-NP (100 mg L^{-1}) was used in order to capture more degradation products. All experiments were conducted at room temperature (22 ± 2 °C) and in the dark. During each experimental process, 1.0 ml sample was withdrawn at certain time intervals and immediately mixed with 0.1 ml methanol to quench ·OH and then was centrifuged at 13,400 rpm for 5 min to separate Fe_3O_4 particles. Finally, the supernatant liquid was collected for analysis.

2.4. Analytical methods

Quantitative analysis of p-NP was carried out by high performance liquid chromatography (HPLC), an Agilent HP-1100 HPLC system equipped with a diode array UV–Vis detector (DAD). An Ultra C_{18} column (5 μm, 4.6 × 250 mm) was used for the separation. The mobile phase was a mixture of methanol and water (60/40, v/v) at a flow rate of 1.0 ml min^{-1}, the injection volume was 20 μl, the temperature of the column chamber was 30 °C, and the detector was operated at 320 nm.

The concentration of dissolved ferrous ion and total iron were measured by colorimetric determination with 1,10-phenanthroline according to the standard method [23], and the absorbance was measured at 510 nm by a Lambda 35 UV/Vis spectrophotometer (Perkin-Elmer, USA) with a 1 cm path length spectrometric quartz cell. The concentration of hydrogen peroxide was determined by the iodide method, and the absorbance was measured at 352 nm (detection limit of ~10^{-6} M) [24].

The aromatic intermediates were identified by high performance liquid chromatography–mass spectrometry (HPLC–MS) and gas chromatography–mass spectrometry (GC–MS). HPLC–MS analysis was performed by an Agilent 1200 HPLC system coupled to 6130 quadrupole mass spectrometer. An Agilent ZORBAX Eclipse XDB-C_{18} column (5 μm, 4.6 × 150 mm) was used for separation. The mobile phase was a mixture of methanol and pH 3.0 formic acid aqueous solution (40/60, v/v) at a flow rate of 0.5 ml min^{-1}, the injection volume was 20 μl, and the temperature of the column chamber was 30 °C. The MS detector was operated with selected ion monitoring (SIM) in negative mode. The operational conditions were as follows: frag-mentor 90, drying gas flow rate 12 l min^{-1}, nebulizer pressure 45 Psig, dry gas temperature 300 °C, vaporizer temperature 150 °C, capillary voltage 2500 V, corona current 4 μA and charging voltage 2000 V.

GC–MS analysis was performed by an Agilent 6890N GC system coupled to a 5973 mass selective detector. 5 ml of samples were withdrawn at 2 h interval and immediately extracted with 3 ml of ethyl acetate and dichloromethane for two times, respectively. The extracts were dried by anhydrous sodium sulfate and then concentrated by nitrogen gas blowing to 0.5 ml. A HP-5MS column (30 m × 250 μm × 0.25 μm) was used for separation. The injector temperature was 280 °C; the column was initiated at 50 °C and held for 5 min, then increased to 300 °C at a rate of 15 °C min^{-1} and then held for 5 min. The carrier gas (Helium) flow rate was 1.2 ml min^{-1}. The samples were injected in the splitless mode and each injection was 1.0 μl. The MS detector was operated in a full scan mode.

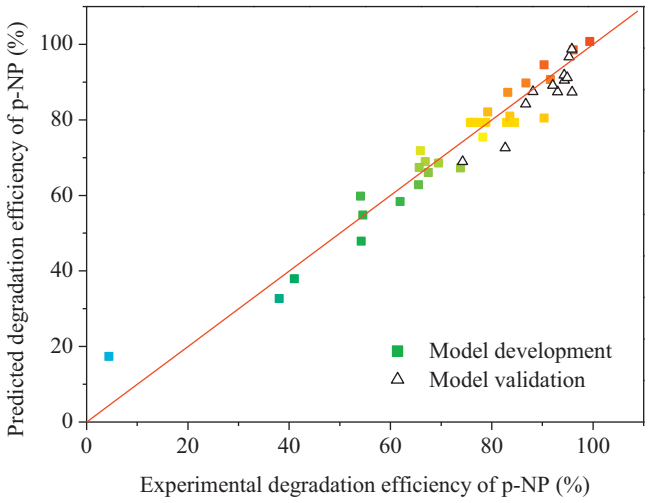

Fig. 1. Comparison of the model predicted degradation efficiencies of p-NP and the experimental values.

3. Results and discussion

3.1. Statistical analysis of the derived response surface model

A total of 30 batch experiments were carried out to develop the response surface model according to the experimental design previously discussed (results are shown in Table S1 of Supporting Information). Eq. (3) shows the derived quadratic polynomial model which represents an empirical relationship between the degradation efficiency of p-NP at 10 h reaction time and the independent input variables.

$$Y(\%) = 79.28 + 5.30x_1 + 15.79x_2 - 8.33x_3 + 0.89x_4 - 2.22x_1^2 - 7.59x_2^2 + 1.20x_3^2 - 1.41x_4^2 + 0.89x_1x_2 + 3.60x_1x_3 + 3.04x_1x_4 + 1.82x_2x_3 + 1.38x_2x_4 + 0.93x_3x_4 \quad (3)$$

Statistical testing of the model was performed by analysis of variance (ANOVA) and the results for the coded variable levels are shown in Table 2. ANOVA analysis indicated that the calculated F value of 18.13 was much larger than the critical value of 2.42 for $F_{0.05}(14,15)$, implying that the derived quadratic polynomial model is significant. In addition, the model correlation coefficient of $R^2 = 0.9442$ suggests that there is good agreement between the experimental and predicted values of the degradation efficiency of p-NP. As shown in Fig. 1, the squares represent the experiments for the model development and the triangles represent the additional experiments for the model validation. It can be seen that the predicted degradation efficiency of p-NP agrees well with the experimental values, with an average relative error of 3.83%. The derived model is adequate to perform the process variables optimization for the degradation of p-NP. The significance of each independent variable was evaluated according to its P-value (a P-value lower than 0.05 indicates that the term is significant at 95% confidence level). The results indicate that the degradation efficiency of p-NP is significantly affected by nano-Fe_3O_4 dosage, hydrogen peroxide concentration and the initial pH; while the initial concentration of p-NP in the studied range (5–45 mg L^{-1}) has a slight effect on the degradation efficiency of p-NP.

3.2. Response surface optimization

Fig. 2A shows the response surface modeling in a three dimensional (3D) representation of the effect of initial pH on the degradation of p-NP by heterogeneous Fenton-like reactions on nano-Fe_3O_4. The pH of the medium is a crucial operating parameter

Table 2
ANOVA analysis of the derived response surface model.[a]

Source	Sum of squares	Degree of freedom	Mean square	*F* value	*P*-value	
Model	10593.82	14	756.7012	18.12697	<0.0001	Significant
X_1: Fe_3O_4	674.372	1	674.372	16.15476	0.0011	
X_2: H_2O_2	5980.621	1	5980.621	143.2673	<0.0001	
X_3: pH	1665.334	1	1665.334	39.8935	<0.0001	
X_4: $C_{p\text{-}NP}$	19.11735	1	19.11735	0.457961	0.5089	
$X_1 \cdot X_2$	12.6736	1	12.6736	0.303599	0.5897	
$X_1 \cdot X_3$	206.7844	1	206.7844	4.953574	0.0418	
$X_1 \cdot X_4$	147.9872	1	147.9872	3.545072	0.0793	
$X_2 \cdot X_3$	53.1441	1	53.1441	1.273081	0.2769	
$X_2 \cdot X_4$	30.63622	1	30.63622	0.733899	0.4051	
$X_3 \cdot X_4$	13.80122	1	13.80122	0.330612	0.5738	
X_1^2	135.2805	1	135.2805	3.240679	0.0920	
X_2^2	1580.455	1	1580.455	37.8602	<0.0001	
X_3^2	39.196	1	39.196	0.93895	0.3479	
X_4^2	54.49852	1	54.49852	1.305526	0.2711	
Residual	626.1673	15	41.74449			
Lack of fit	560.0572	10	56.00572	4.235788	0.0623	Not significant
Pure error	66.11015	5	13.22203			
Cor total	11219.98	29				

[a] $R^2 = 0.9442$, adjusted $R^2 = 0.8921$.

for heterogeneous Fenton-like reactions, which directly affects not only the catalytic performance but also the extent of Fe leaching from the catalysts [25]. The optimal pH for heterogeneous Fenton-like reactions is generally reported to be around 3.0. Since actual industrial wastewater often has a pH around 7.0, initial pH values ranging from 5.0 to 9.0 were investigated in the present study. As shown in Fig. 2A, a negative effect of increasing the initial pH on the degradation of p-NP was observed. This can be explained by the fact that basic conditions lead to the catalytic decomposition of more hydrogen peroxide to O_2 and H_2O on the nano-Fe_3O_4 surface via non-radical producing pathways, but not to the generation of •OH. This point was further confirmed by the interaction effect of the initial pH and hydrogen peroxide dosage on the degradation of p-NP (Fig. 2B), which clearly indicates that the optimum hydrogen peroxide dosage was increased with initial pH increasing. In addition, it has been reported that the oxidation potential of the ·OH at basic conditions is smaller than that at acidic conditions (Eqs. (4) and (5)) [26].

$$\cdot OH + e^- + H^+ \rightarrow H_2O \quad E^o = 2.7/2.38 \ \text{V} \tag{4}$$

$$\cdot OH + e^- \rightarrow OH^- \quad E^o = 1.8 \ \text{V} \tag{5}$$

Moreover, the isoelectric point (IEP) of Fe_3O_4 is normally at pH 6.5–6.8 [27,28]; thus the Fe_3O_4 surface is presumable negatively charged under basic conditions. The pK_a value of p-NP is 7.08 at 22 °C; thus p-NP is also negatively charged under basic conditions. Therefore, the adsorption of p-NP onto the Fe_3O_4 surface can be inhibited under basic conditions due to electrostatic repulsion, which also correspondingly slows down the degradation of p-NP.

The interaction effect of nano-Fe_3O_4 dosage and initial pH on the degradation of p-NP is presented in Fig. 2C. By increasing the catalyst dosage, higher reaction rates and performances are expected

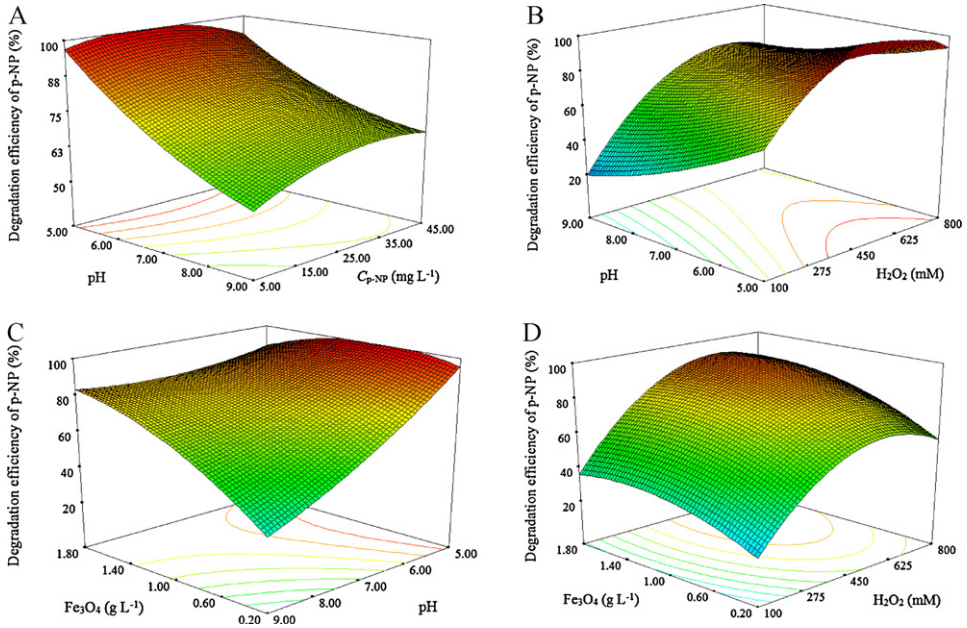

Fig. 2. The 3D response surface plot and contour plot of the degradation efficiency of p-NP as a function of (A) initial pH with initial concentration of p-NP at $[Fe_3O_4]_0 = 1.0\,g\,L^{-1}$, $[H_2O_2]_0 = 400\,mM$, temperature = 22 ± 2 °C and reaction time 10 h; (B) initial pH with H_2O_2 dosage at $[C_{p\text{-}NP}]_0 = 25\,mg\,L^{-1}$, $[Fe_3O_4]_0 = 1.0\,g\,L^{-1}$, temperature = 22 ± 2 °C and reaction time 10 h; (C) Fe_3O_4 dosage with initial pH at $[C_{p\text{-}NP}]_0 = 25\,mg\,L^{-1}$, $[H_2O_2]_0 = 400\,mM$, temperature = 22 ± 2 °C and reaction time 10 h; and (D) H_2O_2 dosage with Fe_3O_4 dosage at $[C_{p\text{-}NP}]_0 = 25\,mg\,L^{-1}$, pH = 7.0, temperature = 22 ± 2 °C and reaction time 10 h.

because it increases the decomposition rate of hydrogen peroxide, hence increasing •OH production [25]. However, an insignificant impact of increasing nano-Fe_3O_4 dosage on the degradation efficiency of p-NP was observed at a low level of initial pH; while at a high level of initial pH, the degradation efficiency of p-NP was significantly improved by increasing nano-Fe_3O_4 dosage. The results demonstrate that 0.6 g L^{-1} nano-Fe_3O_4 is sufficient to obtain a good degradation efficiency of p-NP for the contaminated water with an initial pH of 5.0; while a large dosage of nano-Fe_3O_4 (1.8 g L^{-1}) is suggested for contaminated water with an initial pH of 8.0–9.0. The interaction effect of nano-Fe_3O_4 dosage and hydrogen peroxide dosage on the degradation of p-NP at neutral pH conditions is presented in Fig. 2D. At a constant hydrogen peroxide concentration, a positive effect of increasing nano-Fe_3O_4 dosage on the degradation efficiency of p-NP was observed. With a dosage of nano-Fe_3O_4 larger than 1.5 g L^{-1}, the increase of the degradation efficiency of p-NP was not significant. The optimum hydrogen peroxide dosage was observed at 600–650 mM. Below the optimum dosage, increasing hydrogen peroxide dosage favors the degradation of p-NP which can be attributed to the increase in the yield of •OH. Beyond the optimum dosage, however, the scavenging of ·OH by excessive hydrogen peroxide will became more significant [29] and cause the degradation efficiency and rate of p-NP to decrease. Based on the model prediction, the optimum conditions for the degradation of p-NP by heterogeneous Fenton-like reactions on nano-Fe_3O_4 were determined to be 1.5 g L^{-1} Fe_3O_4, 620 mM H_2O_2, pH 7.0 and 25–45 mg L^{-1} p-NP. The experimental degradation efficiencies of p-NP were greater than 90% under the optimum conditions, which agreed well with the model predicted values (Fig. 1).

Additionally, the strategy of hydrogen peroxide addition is another important issue for the Fenton and Fenton-like process. Generally, hydrogen peroxide is added in a single-step, such addition may cause self-decomposition of hydrogen peroxide due to high concentrations at the point of injection, and scavenging of ·OH by a large amount of hydrogen peroxide [30]. In order to investigate how the addition modes of hydrogen peroxide influence the performance of heterogeneous Fenton-like reactions on nano-Fe_3O_4, we added hydrogen peroxide by single, two- and three-step addition but kept the total quantity the same. The results showed that the corresponding degradation efficiencies of p-NP were not greatly different and more than 95% of p-NP was degraded after 12 h reaction time for all test cases (Fig. S2).

3.3. Catalytic mechanism and radical identification

To investigate the catalytic mechanism of p-NP by Fenton-like reactions on nano-Fe_3O_4 at neutral pH conditions, the first step was to rule out a major contribution of reduction of p-NP by nano-Fe_2O_3. Control experiments showed that the reduction of p-NP by nano-Fe_3O_4 was not significant in the present study (data not shown). The next step was to distinguish the contributions of homogeneous and heterogeneous reactions. Over the course of a typical experiment, the concentration of Fe^{2+} and total dissolved iron was always lower than 0.6 μM and 4.0 μM, respectively (Fig. S3A). Because the activation of hydrogen peroxide by dissolved iron has been observed at concentrations as low as 0.42 μM Fe^{3+} [31], the dissolved iron in the aqueous solution phase might contribute to the degradation of p-NP. To verify that this was not the case, an extra sample of the slurry (without the addition of methanol to quench •OH) was collected at time interval, centrifuged to remove the nano-Fe_3O_4 particles, and analyzed over time for degradation of p-NP. As can be seen in Figure S3B, the results show that after a period of 30 h, the final concentration of p-NP in each unquenched and centrifuged sample was less than 10% lower than when it was first taken and centrifuged, showing minimal, if any, aqueous p-NP degradation. Therefore, it can be concluded that the dissolved iron was unimportant to the degradation of p-NP which mainly occurred by nano-Fe_3O_4 surface-catalyzed, i.e. heterogeneous, reaction.

Previous studies have suggested that the surface-catalyzed decomposition of hydrogen peroxide on iron oxides has a similar mechanism to the traditional Haber–Weiss mechanism, i.e., the degradation of organic contaminants can be attributed to the generation of •OH [31–34]. The ratio of the consumed hydrogen peroxide to the degraded p-NP was 1450:1 (Fig. S3), which indicated that the stoichiometry of the generation of ·OH by the reaction between magnetite and hydrogen peroxide was not as efficient as that of the standard Fenton reagent. This can be explained by the fact that the decomposition of hydrogen peroxide on the surface of iron oxides may go through non-radical pathways, by which hydrogen peroxide is directly converted to O_2 and H_2O by 2 electron transfer reactions without the generation of ·OH (Eq. (6)) [31].

$$2H_2O_2 \xrightarrow{Fe_3O_4} 2H_2O + O_2 \quad (6)$$

The high concentrations of hydrogen peroxide could promote a series of propagation reactions that produce perhydroxyl radical (•OOH), superoxide radical ($O_2^{\bullet -}$) and hydroperoxide anion (HO_2^-) in addition to •OH [35,36]. •OOH is a weak oxidant that is unreactive in aqueous systems. $O_2^{\bullet -}$ is a weak nucleophile and reductant, which is in equilibrium with •OOH ($pK_a = 4.8$). HO_2^- is a strong nucleophile [36]. Previous studies reported that $O_2^{\bullet -}$ is the primary reactive species for the degradation of carbon tetrachloride by modified Fenton's reagent (with high concentration of hydrogen peroxide > 0.1 M) [36,37]. Wang et al. [38] also reported that $O_2^{\bullet -}$/•OOH are the main reactive radicals for the degradation of Rhodamine B by nano-Fe_3O_4 catalyzed hydrogen peroxide. The primary reactive species for the degradation of p-NP in nano-Fe_3O_4 catalyzed hydrogen peroxide process were identified with specific scavenging experiments. 2-propanol was used as a scavenger for ·OH because of its high reactivity with oxidants ($k_{\bullet OH,\text{2-propanol}} = 3 \times 10^9\ M^{-1}\ s^{-1}$) but low reactivity with reductants ($k_e = 1 \times 10^6\ M^{-1}\ s^{-1}$) [37]. In addition, chloroform was used as a scavenger for $O_2^{\cdot -}$ because of its high reactivity with reductants ($k_e = 3 \times 10^{10}\ M^{-1}\ s^{-1}$) but low reactivity with oxidants ($k_{\bullet OH,\text{chloroform}} = 7 \times 10^6\ M^{-1}\ s^{-1}$) [37]. The results showed that the degradation of p-NP was significantly inhibited by the addition of 2-propanol (Fig. 3). The degradation efficiency of p-NP was decreased with a concentration increase of 2-propanol; more than 50% decrease in the degradation efficiencies of p-NP was observed after 12 h reaction time when the mole ratio of 2-propanol to p-NP was larger than 200:1. On the contrary, the addition of chloroform almost did not affect the degradation of p-NP. Although a 10% decrease in the degradation efficiencies of p-NP was observed with the addition of chloroform at a molar ratio of 400:1, this is because the added chloroform dosage was higher than its solubility in water (67 mM, 20 °C), thus some p-NP partitioned from the water phase to the chloroform phase, inhibiting its degradation. Based on the results, it can be concluded that •OH is the primary reactive species for the degradation of p-NP by the nano-Fe_3O_4 catalyzed hydrogen peroxide process.

3.4. Degradation kinetics of p-NP

The degradation kinetics of p-NP by heterogeneous Fenton-like reactions on nano-Fe_3O_4 was investigated at different initial concentrations of p-NP (Fig. 4). The decrease of p-NP concentration versus reaction time in the first 10 h is linear ($R^2 > 0.99$) and linearly increases with an increase of initial concentration of p-NP from 15 to 45 mg L^{-1} (insert in Fig. 4, which shows the degradation rate of p-NP at different initial concentrations). Since ·OH is quite reactive, it rapidly reacts with p-NP ($k_{\bullet OH,\text{p-NP}} = 3.8 \times 10^9\ M^{-1}\ s^{-1}$) [39], H_2O_2 ($k_{\bullet OH,H2O2} = 1.2–4.5 \times 10^7\ M^{-1}\ s^{-1}$) and other radical sink species

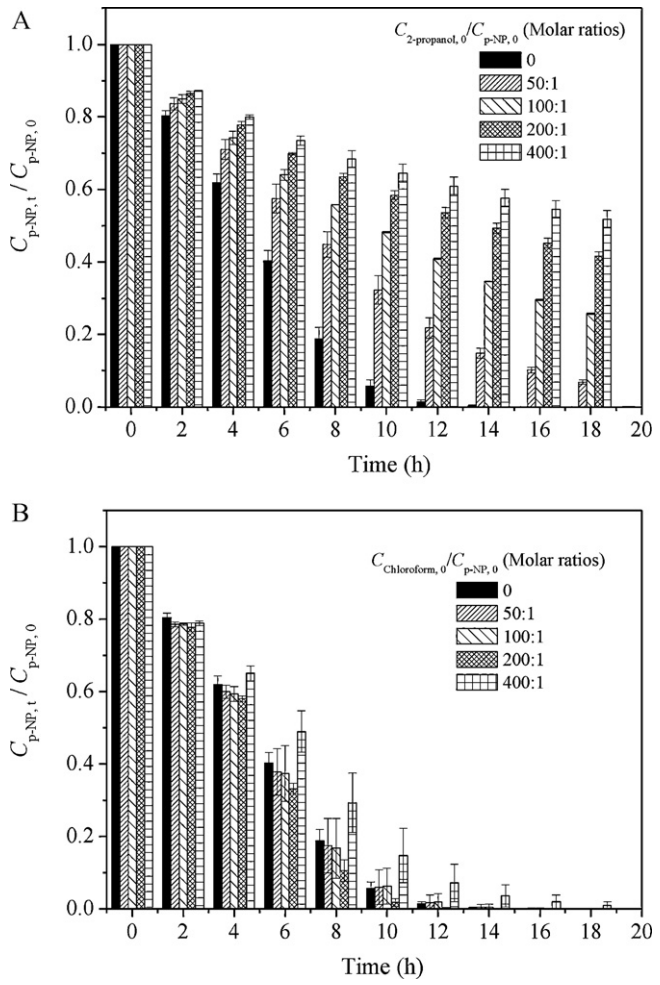

Fig. 3. Effect of •OH scavenger 2-propanol (A) and $O_2^{\bullet-}$ scavenger chloroform (B) on the degradation of p-NP by a nano-Fe_3O_4 catalyzed H_2O_2 process. Experimental conditions: $[C_{p\text{-NP}}]_0 = 25\ mg\ L^{-1}$, $[Fe_3O_4]_0 = 1.5\ g\ L^{-1}$, $[H_2O_2]_0 = 620\ mM$, pH = 7.0 and temperature = 22 ± 2 °C.

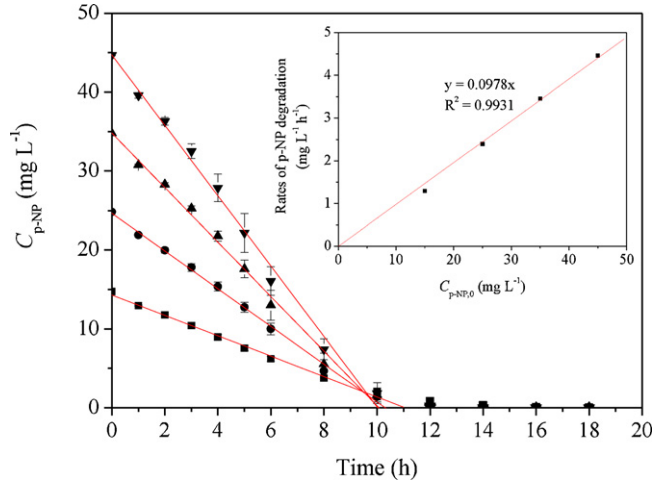

Fig. 4. Degradation kinetics of p-NP by heterogeneous Fenton-like reactions on nano-Fe_3O_4 at different initial concentrations. Experimental conditions: $[Fe_3O_4]_0 = 1.5\ g\ L^{-1}$, $[H_2O_2]_0 = 620\ mM$, pH = 7.0 and temperature = 22 ± 2 °C.

($\sim 10^7$–$10^{10}\ M^{-1}\ s^{-1}$) [40]. •OH would be completely consumed on the nano-Fe_3O_4 surface before diffusing to the bulk solution because the reaction rates of ·OH are much faster than its diffusion rate ($2 \times 10^{-5}\ cm^2\ s^{-1}$) [41]. Therefore, it can be assumed that the degradation of p-NP occurred only by reactions on the surface. Table S3 shows the possible reactions for the degradation of p-NP by heterogeneous Fenton-like reactions on nano-Fe_3O_4. The removal rate of p-NP in aqueous solutions can be presented as Eq. (7),

$$\frac{d[\text{p-NP}]}{dt} = -k_1[\text{p-NP}][Fe_3O_4] + k_{1,R}[\text{p-NP}]_s \quad (7)$$

where k_1 and $k_{1,R}$ are the adsorption and desorption rate constants of p-NP on nano-Fe_3O_4 surface, respectively. The kinetic equation of surface concentration of p-NP is expressed as Eq. (8),

$$\frac{d[\text{p-NP}]_s}{dt} = k_1[\text{p-NP}][Fe_3O_4] - k_{1,R}[\text{p-NP}]_s - k_{\cdot\text{OH,p-NP}}[\text{p-NP}]_s[\cdot\text{OH}]_s \quad (8)$$

Assuming the steady-state surface concentration of p-NP, i.e. $d[\text{p-NP}]_s/dt = 0$, the following expression is obtained,

$$[\text{p-NP}]_s = \frac{k_1[\text{p-NP}][Fe_3O_4]}{k_{1,R} + k_{\cdot\text{OH,p-NP}}[\cdot\text{OH}]_s} \quad (9)$$

If Eq. (9) is substituted into Eq. (7), we obtain the following expression.

$$\frac{d[\text{p-NP}]}{dt} = -\frac{k_1 k_{\cdot\text{OH,p-NP}}[\text{p-NP}][Fe_3O_4]}{k_{1,R}/[\cdot\text{OH}]_s + k_{\cdot\text{OH,p-NP}}} \quad (10)$$

According to Eq. (10), the removal rate of p-NP in aqueous solutions is directly proportional to p-NP concentration in aqueous solutions, nano-Fe_3O_4 concentration and surface concentration of ·OH, the second order reaction rate constant, $k_{\bullet\text{OH, p-NP}}$, and the adsorption rate constant of p-NP on the nano-Fe_3O_4 surface, k_1; and inversely proportional to the desorption rate constant of p-NP on the nano-Fe_3O_4 surface, $k_{1,R}$. At a constant amount of nano-Fe_3O_4 and surface concentration of •OH, the removal rate of p-NP in aqueous solutions would follow pseudo-first-order degradation kinetics. As shown in Fig. 4, however, a constant degradation rate of p-NP in aqueous solutions suggests that the surface concentration of •OH increases with the decrease of p-NP concentration.

The decomposition pathways of the adsorbed hydrogen peroxide on the nano-Fe_3O_4 surface include a radical producing pathway and a non-radical producing pathway; thus the generation rate of •OH ($V_{\bullet\text{OH}}$) is expressed as Eq. (11),

$$V_{\cdot\text{OH}} = k_{\equiv Fe^{2+},H_2O_2}[\equiv Fe^{2+}] \cdot \eta[H_2O_2]_s \quad (11)$$

where η is the effectiveness factor, which represents the ratio of the surface adsorbed hydrogen peroxide that goes through the radical producing pathway to the total surface adsorbed hydrogen peroxide concentration. The factors that control the $V_{\bullet\text{OH}}$ include the concentration of $\equiv Fe^{2+}$, which is proportional to the nano-Fe_3O_4 dosage; the surface concentration of hydrogen peroxide; and the η value. Because $\equiv Fe^{2+}$ would be rapidly oxidized to $\equiv Fe^{3+}$ according to reaction 4 (R4) in Table S3 of Supporting Information, the concentration of $\equiv Fe^{2+}$ is thus expected to be decreased, although it could be regenerated by reaction 5 (R5) (the reaction rate of R5 is much smaller than that of R4, Table S3). In addition, the rate-dominating step of the heterogeneous reaction, either the rate of intrinsic chemical reactions on the iron oxide surface or the diffusion rate of the solutes to the surface, can be estimated by Eq. (12) [32].

$$\varphi = \sqrt{\frac{k}{D/L^2}} \quad (12)$$

where k is the first order reaction rate constant of hydrogen peroxide, $1.03 \times 10^{-5}\ s^{-1}$; D is the diffusion coefficient of hydrogen

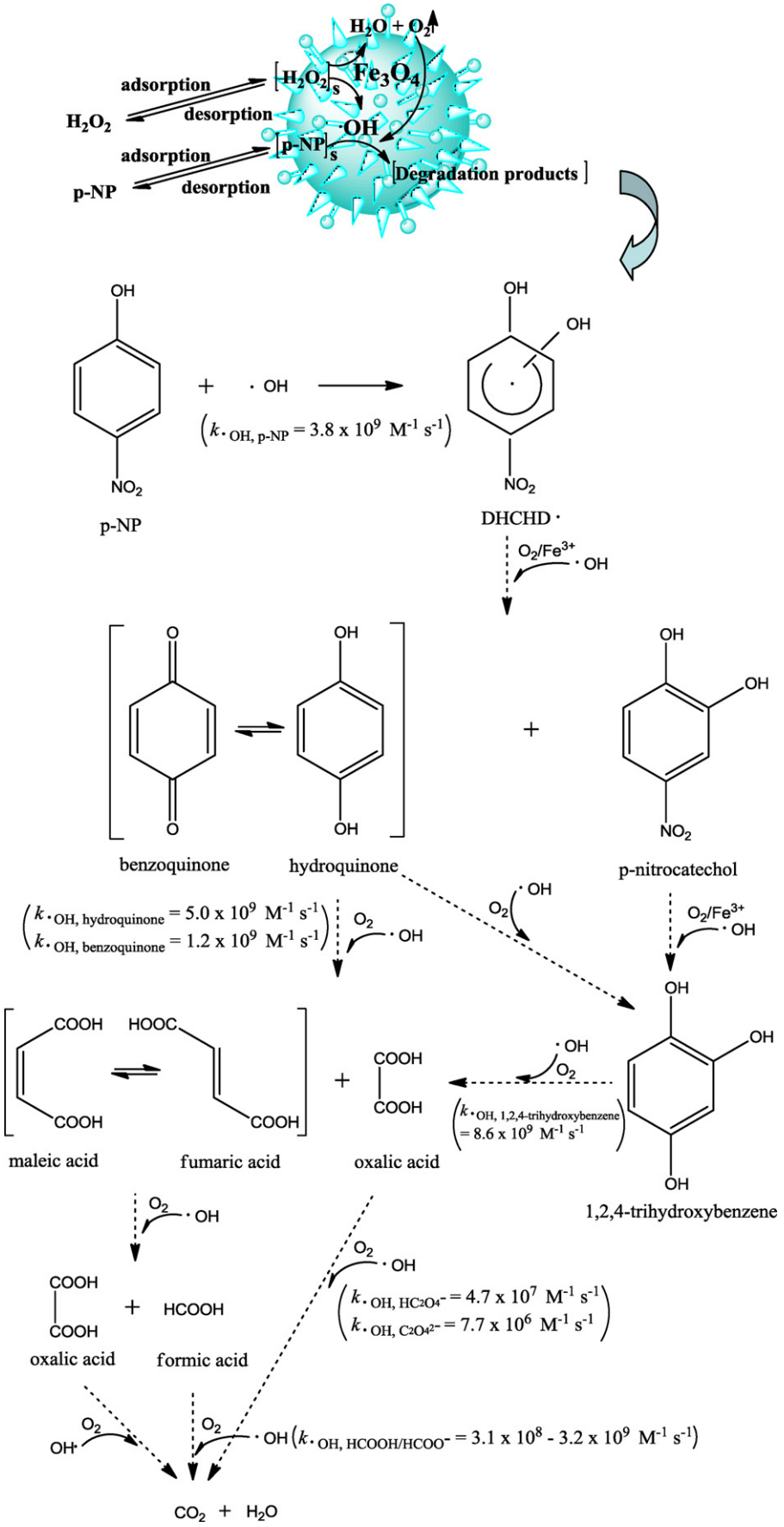

Fig. 5. Proposed reaction mechanisms of the degradation of p-NP by heterogeneous Fenton-like reactions on nano-Fe_3O_4.

peroxide in water, 1.4×10^{-5} cm^2 s^{-1} [42]; and L is the thickness of the stagnant liquid film, $\sim 10^{-3}$ cm [32]. The value was calculated to be 8.58×10^{-4} (<0.5), implying that the diffusion rate of hydrogen peroxide through the external film to the nano-Fe_3O_4 surface is much faster than its reaction rate on the surface. As a result, the adsorption and desorption of hydrogen peroxide on nano-Fe_3O_4 surface is fast enough to reach a pseudo-equilibrium and the intrinsic reactions of hydrogen peroxide on nano-Fe_3O_4 surface are expected to be the rate-limiting steps. Because the decrease of hydrogen peroxide concentration in aqueous solution and the loss of adsorption site on the nano-Fe_3O_4 surface by the competition of degradation intermediates would lead to the decrease of the equilibrium surface concentration of hydrogen peroxide, the increase of the surface concentration of •OH is most likely to relate to the increase of η value according to Eq. (11). This can be explained by the fact that the non-radical producing pathway is the predominant route of hydrogen peroxide decomposition on the nano-Fe_3O_4 surface at high pH. However, the formation of short chain carboxylic acids gradually decreases the solution pH (Fig. S3), which correspondingly enhances hydrogen peroxide decomposition via a radical producing pathway. Therefore, it could be proposed that the η value increased as a function of the decrease of the solution pH. The decrease of oxygen production rates as a function of the decrease of pH from 7.0 to 4.0 was also observed in a goethite-catalyzed hydrogen peroxide process [43]. Moreover, the generation rate of ·OH should be equal to its scavenging rate:

$$V_{\cdot OH} = k_{\cdot OH,p\text{-}NP}[p\text{-}NP]_s[\cdot OH]_s + \sum_j k_{\cdot OH,S_j}[S_j]_s[\cdot OH]_s \quad (13)$$

where S_j are the scavenger species, including the degradation intermediates, $\equiv Fe^{2+}$, H_2O_2, $O_2^{\bullet -}$/•OOH and •OH itself. If Eq. (13) is substituted into Eq. (11), we can obtain the following expression.

$$[\cdot OH]_s = \frac{\eta k_{\equiv Fe^{2+},H_2O_2}[\equiv Fe^{2+}][H_2O_2]_s}{k_{\cdot OH,p\text{-}NP}[p\text{-}NP]_s + \sum_j k_{\cdot OH,S_j}[S_j]_s} \quad (14)$$

According to Eq. (14), the surface concentration of ·OH is directly proportional to the η value. It is noteworthy that η is not only as a function of pH condition, but also may relate to the formed complexes on the nano-Fe_3O_4 surface by the degradation intermediates. It has been reported that the degradation products of many aromatic compounds are capable of complexing iron [9], which possibly interferes with the decomposition pathway of hydrogen peroxide on the nano-Fe_3O_4 surface; thus further studies are needed to explore the interactions between degradation products and nano-Fe_3O_4.

3.5. Degradation pathways of p-NP

The aromatic intermediates were identified by LC–MS and GC–MS. Benzoquinone ($[M-H]^-$ m/z 107, retention time (RT) of 3.161 min), hydroquinone ($[M-H]^-$ m/z 109, RT 3.098 min), 1,2,4-trihydroxybenzene ($[M-H]^-$ m/z 125, RT 3.227 min), p-nitrocatechol ($[M-H]^-$ m/z 154, RT 8.653 min) and one unidentified product (RT 6.181 min) were detected by LC–MS analysis. Only benzoquinone (RT 7.471 min) was detected by GC–MS analysis, probably due to the concentration of intermediates which was too low to be extracted by the liquid-liquid extraction method. The identified intermediates were in agreement with some works on the degradation of p-NP by other kinds of AOPs. Benzoquinone, hydroquinone, 1,2,4-trihydroxybenzene, p-nitrocatechol and p-nitropyrogallol were identified in the degradation of p-NP by an electro-Fenton process [2]. Hydroquinone, 1,2,4-trihydroxybenzene, p-nitrocatechol and p-nitropyrogallol were identified in the degradation of p-NP by a UV/H_2O_2 process [44]. Additionally, hydroquinone, 1,2,4-trihydroxybenzene and p-nitrocatechol were identified in the degradation of p-NP by TiO_2 photocatalytic process [45]. Based on the identified major aromatic intermediates, the possible degradation scheme of p-NP by nano-Fe_3O_4 catalyzed hydrogen peroxide process was proposed (Fig. 5). Firstly, •OH was generated by the catalytic decomposition of absorbed hydrogen peroxide on the nano-Fe_3O_4 surface. The degradation of absorbed p-NP was initiated by the attack of •OH, and dihydroxycyclohexadienyl radical (DHCHD•) was initially formed [2]. Secondly, DHCHD· was then rapidly oxidized to hydroxylated derivatives in the presence of oxidizing agents such as O_2 and Fe^{3+}. Because the mesomeric electro donor character of the hydroxyl group (–OH) on the benzene ring favors the electrophilic attack of ·OH on *ortho*- and *para*-positions with respect to –OH [2,46], hydroquinone (which is capable of being rapidly oxidized to benzoquinone in oxidation circumstances) and p-nitrocatechol were, therefore, primarily formed during the oxidation of DHCHD•. The formation of 1,2,4-trihydroxybenzene can be explained by the electrophilic attack of •OH on hydroquinone and/or by the *ipso*-attack of •OH on the $-NO_2$ of p-nitrocatechol. Thirdly, the aromatic intermediates were further oxidized by •OH to form short chain carboxylic acids such as fumaric acid, oxalic acid and formic acid, etc., which resulted in the rapid decrease of solution pH (Fig. S4). Furthermore, a slight increase of the solution pH was observed after the complete degradation of p-NP which can be explained by the formation of short chain carboxylic acids that were further oxidized by •OH to CO_2 and H_2O. It has been reported that formic acid can rapidly react with •OH, $k_{\bullet OH,HCOOH/HCOO^-} = 3.1 \times 10^8 - 3.2 \times 10^9$ M^{-1} s^{-1} [47]; however, oxalic acid is less reactive towards •OH, $k_{\bullet OH,C2O4^{2-}} = 7.7 \times 10^6$ M^{-1} s^{-1} and $k_{\bullet OH,HC2O4^-} = 4.7 \times 10^7$ M^{-1} s^{-1} [48].

4. Conclusions

The successful degradation of p-NP in water with initial neutral pH was achieved by the heterogeneous catalytic decomposition of hydrogen peroxide on nano-Fe_3O_4. The major aromatic intermediates including benzoquinone, hydroquinone, 1,2,4-trihydroxybenzene and p-nitrocatechol were also rapidly degraded by the attack of •OH and did not accumulate after treatment. In addition, the concentration of leaching iron was lower than 0.25 mg L^{-1}, whereas the maximum contaminant level standard for iron in drinking water is 0.3 mg L^{-1}, US EPA. It is easy to remove nano-Fe_3O_4 from aqueous solutions by magnetic separation and the generation of iron sludge can be avoided. Therefore, this process can be considered as an environmentally benign technology for the remediation of p-NP and other agrochemical contaminated water and soil. Furthermore, the results indicate that CCD coupled with RSM is a useful technique to optimize the important parameters of heterogeneous Fenton-like reactions on nano-Fe_3O_4 for p-NP degradation. This study has important implications for the design of experiments, experimental assays and fitting of results using mathematical methods in multivariable systems.

Acknowledgments

The study was funded in part by the College of Human Ecology, Cornell University and in part by the Cornell University Agricultural Experiment Station federal formula funds, Project No. NYC-329806 (W-1045), received from the Cooperative State Research, Education, and Extension Service, U.S. Department of Agriculture. Any opinions, findings, conclusions, or recommendations expressed in

this publication are those of the author(s) and do not necessarily reflect the views of the U.S. Department of Agriculture.

Appendix A. Supplementary data

Supplementary data associated with this article can be found, in the online version, at doi:10.1016/j.molcata.2011.08.022.

References

[1] U.S. EPA. http://www.epa.gov/ne/npdes/permits/generic/prioritypollutants.pdf.
[2] M.A. Oturan, J. Peiroten, P. Chartrin, A.J. Acher, Environ. Sci. Technol. 34 (2000) 3474–3479.
[3] R.J. Watts, B.C. Bottenberg, T.F. Hess, M.D. Jensen, A.L. Teel, Environ. Sci. Technol. 33 (1999) 3432–3437.
[4] R. Matta, K. Hanna, S. Chiron, Sci. Total Environ. 385 (2007) 242–251.
[5] S. Navalon, M. Alvaro, H. Garcia, Appl. Catal. B: Environ. 99 (2010) 1–26.
[6] X. Zeng, A.T. Lemley, J. Agric. Food Chem. 57 (2009) 3689–3694.
[7] Y. Zhao, J. Hu, W. Jin, Environ. Sci. Technol. 42 (2008) 5277–5284.
[8] Y. Flores, R. Flores, A.A. Gallegos, J. Mol. Catal. A: Chem. 281 (2008) 184–191.
[9] W.P. Kwan, B.M. Voelker, Environ. Sci. Technol. 37 (2003) 1150–1158.
[10] C.A. Gorski, J.T. Nurmi, P.G. Tratnyek, T.B. Hofstetter, M.M. Scherer, Environ. Sci. Technol. 44 (2009) 55–60.
[11] K.M. Danielsen, K.F. Hayes, Environ. Sci. Technol. 38 (2004) 4745–4752.
[12] W. Lee, B. Batchelor, Environ. Sci. Technol. 36 (2002) 5147–5154.
[13] M.L. Ferrey, R.T. Wilkin, R.G. Ford, J.T. Wilson, Environ. Sci. Technol. 38 (2004) 1746–1752.
[14] E.K. Nefso, S.E. Burns, C.J. McGrath, J. Hazard. Mater. 123 (2005) 79–88.
[15] H.A. Wiatrowski, S. Das, R. Kukkadapu, E.S. Ilton, T. Barkay, N. Yee, Environ. Sci. Technol. 43 (2009) 5307–5313.
[16] Y.T. He, S.J. Traina, Environ. Sci. Technol. 39 (2005) 4499–4504.
[17] E.S. Ilton, J.-F. Boily, E.C. Buck, F.N. Skomurski, K.M. Rosso, C.L. Cahill, J.R. Bargar, A.R. Felmy, Environ. Sci. Technol. 44 (2010) 170–176.
[18] R.C.C. Costa, F.C.C. Moura, J.D. Ardisson, J.D. Fabris, R.M. Lago, Appl. Catal. B: Environ. 83 (2008) 131–139.
[19] X. Zeng, K. Hanna, A.T. Lemley, J. Mol. Catal. A: Chem. 339 (2011) 1–7.
[20] S. Ghasempur, S.-F. Torabi, S.-O. Ranaei-Siadat, M. Jalali-Heravi, N. Ghaemi, K. Khajeh, Environ. Sci. Technol. 41 (2007) 7073–7079.
[21] M.B. Kasiri, H. Aleboyeh, A. Aleboyeh, Environ. Sci. Technol. 42 (2008) 7970–7975.
[22] R.J. Watts, P.C. Stanton, J. Howsawkeng, A.L. Teel, Water Res. 36 (2002) 4283–4292.
[23] L.S. Clesceri, A.E. Greenberg, A.D. Eaton, M.A.H. Franson, Standard Methods for the Examination of Water and Wastewater, 20th ed., American Public Health Association, 1998.
[24] C. Kormann, D.W. Bahnemann, M.R. Hoffmann, Environ. Sci. Technol. 22 (1988) 798–806.
[25] J. Herney-Ramirez, M.A. Vicente, L.M. Madeira, Appl. Catal. B: Environ. 98 (2010) 10–26.
[26] G.P. Anipsitakis, D.D. Dionysiou, Environ. Sci. Technol. 37 (2003) 4790–4797.
[27] G.A. Parks, Chem. Rev. 65 (1965) 177–198.
[28] S. Laurent, D. Forge, M. Port, A. Roch, C. Robic, L. Vander Elst, R.N. Muller, Chem. Rev. 108 (2008) 2064–2110.
[29] C. Walling, S. Kato, J. Am. Chem. Soc. 93 (1971) 4275–4281.
[30] Y. Deng, J.D. Englehardt, Water Res. 40 (2006) 3683–3694.
[31] A.L.-T. Pham, C. Lee, F.M. Doyle, D.L. Sedlak, Environ. Sci. Technol. 43 (2009) 8930–8935.
[32] S.-S. Lin, M.D. Gurol, Environ. Sci. Technol. 32 (1998) 1417–1423.
[33] W. Luo, L. Zhu, N. Wang, H. Tang, M. Cao, Y. She, Environ. Sci. Technol. 44 (2010) 1786–1791.
[34] X. Xue, K. Hanna, M. Abdelmoula, N. Deng, Appl. Catal. B: Environ. 89 (2009) 432–440.
[35] L.L. Bissey, J.L. Smith, R.J. Watts, Water Res. 40 (2006) 2477–2484.
[36] B.A. Smith, A.L. Teel, R.J. Watts, Environ. Sci. Technol. 38 (2004) 5465–5469.
[37] A.L. Teel, R.J. Watts, J. Hazard. Mater. 94 (2002) 179–189.
[38] N. Wang, L. Zhu, D. Wang, M. Wang, Z. Lin, H. Tang, Ultrason. Sonochem. 17 (2010) 526–533.
[39] F.J. Beltrán, V. Gómez-Serrano, A. Durán, Water Res. 26 (1992) 9–17.
[40] C. Walling, Acc. Chem. Res. 8 (1975) 125–131.
[41] R. Roots, S. Okada, Radiat. Res. 64 (1975) 306–320.
[42] P.S. Stewart, J. Bacteriol. 185 (2003) 1485–1491.
[43] R.J. Watts, M.K. Foget, S.-H. Kong, A.L. Teel, J. Hazard. Mater. 69 (1999) 229–243.
[44] W.B. Zhang, X.M. Xiao, T.C. An, Z.G. Song, J.M. Fu, G.Y. Sheng, M.C. Cui, J. Chem. Technol. Biotechnol. 78 (2003) 788–794.
[45] M.S. Dieckmann, K.A. Gray, Water Res. 30 (1996) 1169–1183.
[46] A. Di Paola, V. Augugliaro, L. Palmisano, G. Pantaleo, E. Savinov, J. Photochem. Photobiol. A: Chem. 155 (2003) 207–214.
[47] W.P. Kwan, B.M. Voelker, Environ. Sci. Technol. 36 (2002) 1467–1476.
[48] M.E. Balmer, B. Sulzberger, Environ. Sci. Technol. 33 (1999) 2418–2424.